Nonuniform Reaction Rates during CO and CO/H_2 Oxidation on Coupled Pt Electrodes†

István Z. Kiss, Andrew W. Brackett, and John L. Hudson*

Department of Chemical Engineering, 102 Engineers' Way, University of Virginia, Charlottesville, Virginia 22904-4741

Received: February 4, 2004; In Final Form: April 20, 2004

The electro-catalytic oxidation of CO and CO/H_2 mixtures on polycrystalline Pt has been investigated on two electrodes with controllable degrees of coupling strength by means of experiments and numerical simulations. With strong positive coupling, large differences between the currents of the two almost-identical electrodes arise in a range of potential. Experiments on CO oxidation were carried out in three different electrolytes; all three electrolytes support pattern formation to an extent in the following order: 0.05 mol/L sulfuric acid with saturated sodium sulfate > 0.05 mol/L sulfuric acid > 0.1 mol/L perchloric acid. Experiments with 2% CO/H_2 mixtures also exhibit nonuniform states with coupling. Numerical simulations on CO electro-oxidation confirmed the experimental findings: the current differences occur due to a symmetry breaking both with identical electrodes (through a pitchfork bifurcation) and with electrodes with inherent heterogeneities (due to a formation of an isola). The nonuniform reaction rates due to small inherent heterogeneities are greatly amplified by coupling. Simulations also show that the total coverage of CO and OH is always lower (and the number of total free active sites higher) in the nonuniform states; this suggests the possibility of increased total reaction rate not only in the CO oxidation system but also in systems in which the CO electro-oxidation occurs in parallel with other chemical and electrochemical reaction steps.

1. Introduction

The irreversible adsorption of CO on Pt and its electro-oxidation have been extensively studied in several contexts including the CO poisoning of low-temperature fuel cells.[1] This reaction has also exhibited kinetic and spatiotemporal dynamical features that could have relevance to both catalyst and cell design. A Langmuir-Hinselwood mechanism, in which adsorbed CO reacts with adsorbed OH to form CO_2, has been proposed to model the kinetics of the reaction.[2] The negative reaction order of CO bulk concentrations[3,4] implies that the reactant, CO, self-inhibits CO_2 formation, resulting in a chemical positive feedback loop—an often necessary requirement for nontrivial dynamical features such as bistability. Indeed, bistability has been found in the electro-oxidation of CO: the reaction rate can be high (mass-transfer controlled) or low[5] at a given electrode potential. Bistable (S-shaped) polarization curves have been reported for various electrolytes including sulfuric acid and perchloric acid on Pt single crystals.[5,6] Koper at al. [6] constructed an ODE model based on charge balance and mass balance equations for surface CO concentration and CO and OH coverages; the model reproduces the experimentally observed bistability with an S-shaped polarization curve.

The CO oxidation system can also exhibit spatial Turing patterns through symmetry breaking.[7] Regular stationary patterns predicted by Turing [8] are far-from-equilibrium phenomena in which differences in diffusion rates of reaction species destabilize the uniform distribution and produce concentration patterns.[9−11] These patterns can occur in activator−inhibitor systems in which the inhibitor diffuses faster than the activator. Thus, patterns can form when the inhibitor species are strongly, and the activator species are weakly, coupled to neighboring reacting sites. In electrochemical systems the interactions are often due to the strong electrical coupling through the conducting electrolyte;[12] Turing patterns are expected to occur when the electrode potential is the inhibitor and chemical species are the activators.[13,14] Such electrochemical systems can exhibit S-shaped polarization curves on uniform surfaces and exhibit electrode-size-independent patterns readily with strong electrical interactions; this idea was first verified in the reduction of periodate on Au electrodes.[15] The electrocatalytic oxidation of CO also exhibits an S-shaped polarization curve and thus is a potential candidate for rich stationary pattern formation; nonuniform stationary potential distributions during CO oxidation on a rotating ring have been recently reported.[7]

The coupling through the electric field in the electrolyte is usually long range. Although both the strength and the length scale of this coupling can be varied by changes in electrolyte resistivity and cell geometry,[12,16] these variations are difficult to make without simultaneously altering the driving force of the reaction. For example, changing the cell geometry changes the potential drop through the electrolyte and thus also the potential drop across the electrical double layer. Circuit resistances also add a global coupling.[12,16] We have been using electrode arrays to explore the effect of coupling strength on electrochemical pattern formation and spatiotemporal dynamics.[17−19] The use of electrode arrays has several positive features: the temporally varying current of each electrode in the array can be easily followed with ammeters so that spatiotemporal patterns are directly measured; furthermore, the electrical interaction strength among the electrodes can be tuned with external resistors. This allows variation in coupling strength without concurrent changes in the reaction terms. Thus, the arrays provide a convenient experimental tool to explore the effect of coupling on electrochemical reaction systems.

† Part of the special issue "Gerhard Ertl Festschrift".

* Corresponding author. E-mail: hudson@virginia.edu.

10.1021/jp0494943 CCC: $27.50
Published on Web 06/12/2004

TABLE 1: Model Constants

constant		value	units
α	Butler−Volmer symmetry coefficient	0.5	unitless
A	electrode area	1	cm^2
$c_{CO,s}$	concentration of CO in the bulk solution	1×10^{-6}	mol/cm^3
C_d	capacitance of double layer	2×10^{-5}	F/cm^2
δ	diffusion layer thickness	6.7×10^{-3}	cm
D	diffusion coefficient	5×10^{-5}	cm^2/s
F	Faraday's constant	96485	C/mol
$k_{CO,ads}$	rate constant for CO adsorption onto the surface	1×10^{-8}	1/s
$k_{OH,ads}$	rate constant for OH adsorption onto the surface	1×10^{-4}	1/s
$k_{OH,des}$	rate constant for OH desorption from the surface	1×10^{5}	1/s
k_r	rate constant for CO reaction on the surface	1×10^{-5}	1/s
R	gas constant	8.314	J/(mol K)
S_{tot}	total catalyst sites available for reaction	2.2×10^{-9}	$1/cm^2$
θ_{OH}^{max}	OH maximum surface coverage	0.333	unitless
T	temperature	298	K

In this paper, symmetry breaking and stationary pattern formation of electrocatalytic CO oxidation on polycrystalline Pt are investigated in a two-electrode setup. The two-electrode studies yield information on the effect of various degrees of coupling strength on the symmetry breaking as well as the effect of heterogeneities. The experimental parameters are chosen to yield conditions where the positive feedback of CO is present although the behavior of a single electrode is mono-stable. The effects of positive coupling on stationary pattern formation are investigated in both experiments and numerical simulations. Conditions are chosen such that interactions through the electrolyte are weak; coupling is added through variations in parallel and series external resistors. The simple two-electrode system elucidates many important features that occur in distributed reacting systems such as structure formation, the symmetry breaking, and variations in reaction rate and surface coverage of adsorbed species. Furthermore, the effect of systematic changes in coupling strength on the pattern formation can be studied. The robustness and generality of the findings are explored in three acidic electrolytes with different sulfate content (0.05 mol/L sulfuric acid with sat. Na_2SO_4, 0.05 mol/L sulfuric acid, and 0.1 mol/L perchloric acid). In the numerical simulations the effect of pattern formation on total reaction rates and fraction of free reacting sites are explored.

The patterns studied here are also expected to occur in systems in which CO oxidation is a sub-process or a side reaction. To explore this idea, patterns are investigated in experiments with 2% CO/H_2 mixtures.

2. Simulations

Model. A detailed model describing the S-shaped polarization curve of CO electro-oxidation on a single Pt electrode has been proposed by Koper et al.[6] The model is based on a dual site Langmuir−Hinshelwood kinetics in which adsorbed CO reacts with adsorbed OH to form CO_2. The reaction takes place through 4 steps:

$$CO^{bulk} \leftrightarrow CO^{surface} \quad \text{(I)}$$

$$CO^{surface} + Pt \rightarrow CO - Pt \quad \text{(II)}$$

$$H_2O + Pt \leftrightarrow OH - Pt + H^+ + e^- \quad \text{(III)}$$

$$CO - Pt + OH - Pt \rightarrow CO_2 + H^+ + e^- \quad \text{(IV)}$$

CO diffuses to the Pt surface (step I) and adsorbs quickly (step II). Adsorbed OH is produced by a dissociative mechanism through step III; CO_2 is produced by the reaction between adsorbed CO and OH (step IV). The rates of steps III and IV which involve charge transfer are dependent on potential. A three-variable ODE model can be constructed [6] to describe the variation of CO coverage (Θ_{CO}), OH coverage (Θ_{OH}), and the surface concentration of CO ($c_{CO,s}$):

$$\frac{d\theta_{CO}}{dt} = v_{CO,ads} - v_{react} \quad \text{(1a)}$$

$$\frac{d\theta_{OH}}{dt} = v_{OH} - v_{react} \quad \text{(1b)}$$

$$\frac{dc_{CO,s}}{dt} = -\frac{2S_{tot}}{\delta} v_{CO,ads} + \frac{2D}{\delta^2}(c_{CO,bulk} - c_{CO,s}) \quad \text{(1c)}$$

where v_{react} and v_{OH} are the CO oxidation and OH adsorption rates, respectively:

$$v_{react} = k_r \theta_{CO} \theta_{OH} \exp(\alpha FE/RT) \quad (2)$$

$$v_{OH} = k_{OH,ads} \exp(\alpha FE/RT)[\theta^{max}_{OH}(1 - \theta_{CO}) - \theta_{OH}] - k_{OH,des} \exp(-(1 - \alpha)FE/RT)\theta_{OH} \quad (3)$$

v_{CO} is the rate of CO adsorption:

$$v_{CO,ads} = k_{CO,ads} c_{CO,s}(0.99 - \theta_{CO} - \theta_{OH}) \quad \text{for } \theta_{CO} + \theta_{OH} \le 0.99 \quad \text{(4a)}$$

$$v_{CO,ads} = 0 \quad \text{for } \theta_{CO} + \theta_{OH} \ge 0.99 \quad \text{(4b)}$$

The CO and OH coverages are limited to 0.99, and $\Theta^{OH}_{max} = 0.33$, respectively; values for other kinetic constants are given in Table 1.[6] The potential drop across the double layer (E) is an important quantity in the system: its value determines the experimentally measurable Faradaic current density, j_F:

$$j_F = FS_{tot}(v_{OH} + v_{react}) \quad (5)$$

The model in its present form is meant only to give a qualitative description of the experimental results. For example, the effect of anions on the adsorption of OH and the rate of CO oxidation is not included. A simplified mass transfer model with a constant diffusion layer thickness is taken. Although such approximations are commonly used, their effect on the detailed behavior of the present system is not known. Nevertheless, as we shall see below, the model does reproduce and help explain the characteristics of pattern formation seen in the experiments.

Figure 1a shows j_F as a function of E. A bistable region is found in which CO oxidation can be fast (upper branch) or slow

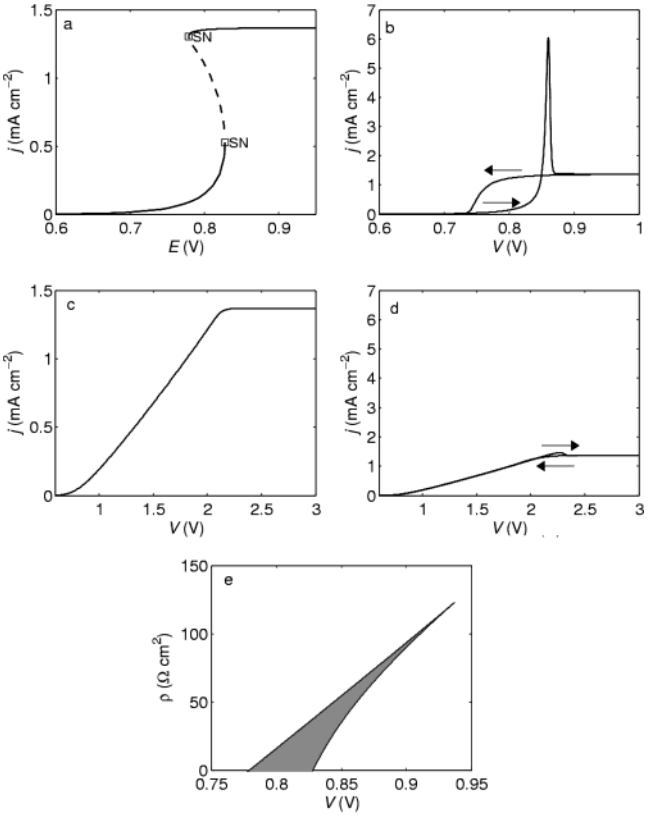

Figure 1. Numerical simulations of the dynamics of a single electrode. (a) Bifurcation diagram showing the current density (j) as a function of the potential drop through the double layer (E). Solid line: stable steady state. Dashed line: unstable steady state. SN: saddle-node bifurcation. (b) Cyclic voltametry scans at $R = 1\ \Omega$. Arrows indicate the direction of the scan. (Scan rate: 50 mV/s) (c) Current vs fixed values of potential at large resistance, $R = 1000\ \Omega$. (d) Cyclic voltammetry scan at $R = 1000\ \Omega$. Scan rate: 50 mV/s. (e) Two-parameter bifurcation diagram showing the bistable region (shaded area) in the ρ vs V plane. $A = 1$ cm^2.

(lower branch) at a given value of E. The bistability here is due to the kinetics since E, the potential drop across the double layer, is fixed. The two stable branches are connected by an unstable branch that exhibits negative differential resistance. The S-shaped curve in Figure 1a is a characteristic feature of CO oxidation and a result of the chemical autocatalytic effect of CO.

In an experiment the potential drop across the double layer (E) cannot be controlled because of an unavoidable potential drop in the electrolyte. Typically, either the overall applied circuit potential (V) or the total current is controlled; here we consider the former case. (A schematic showing the relationship between the potentials V and E for a two-electrode system is given in Figure 2b; the single-electrode case is similar.) The two potentials V and E are related through a charge balance:

$$C_d \frac{dE}{dt} = \frac{V - E}{RA} - j_F \tag{6}$$

where R is the uncompensated resistance of the electrolyte and the external circuitry, C_d is the double layer capacity, and A is the surface area of the electrode. Figure 1b shows the current density ($j = (V - E)/RA$) as a function of the circuit potential during cyclic voltammetry in which the circuit potential is scanned up and down ($dV/dt = \pm$ scan rate) at a small resistance of 1 Ω. Bistability is also seen on the polarization scan; in addition, some transient effects are observed such as the large

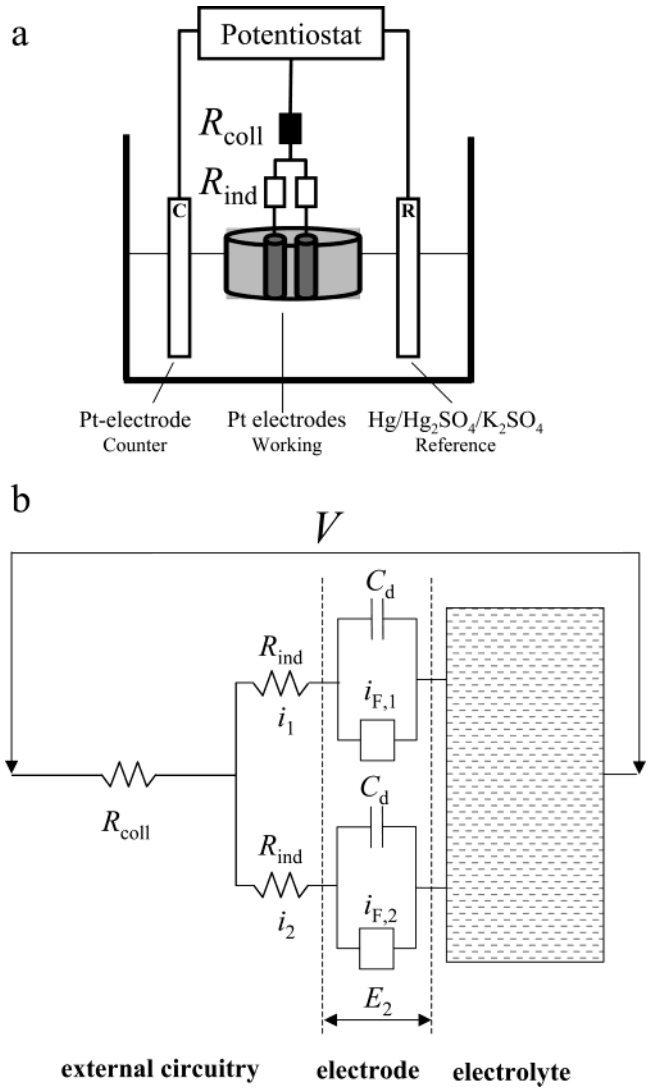

Figure 2. Schematics of two coupled electrodes. (a) Electrochemical cell with a two-electrode array coupled through a combination of collective (R_{coll}) and individual (R_{ind}) resistances. (b) Simplified equivalent circuit.

oxidation peak during the transition from the lower branch to the upper branch.

Current at fixed values of V and with scans in V are shown in Figures 1c and 1d, respectively, with a large circuit resistance (1000 Ω); no bistability is observed at this large resistance and the transient effects are smaller than in the case of small resistance. The region of bistability in the resistivity ($\rho = RA$) − circuit potential (V) plane is shown in Figure 1e; there exists a critical resistivity (in this case about 123 Ω cm^2) above which only a monostable state is seen.

We now consider sets of coupled electrodes. Well-controlled electrical coupling of the electrodes can be implemented with a combination of series (collective, R_{coll}), and parallel (individual, R_{ind}) resistors (see Figure 2a).[20] The coupling strength is varied through changes in the collective resistance fraction

$$\epsilon = R_{coll}/R_{tot} \tag{7}$$

while keeping the total resistance constant:

$$R_{tot} = R_{coll} + R_{ind}/N \tag{8}$$

where N is the number of electrodes. For convenient comparison between arrays of different sizes an equivalent resistance R_{eq}

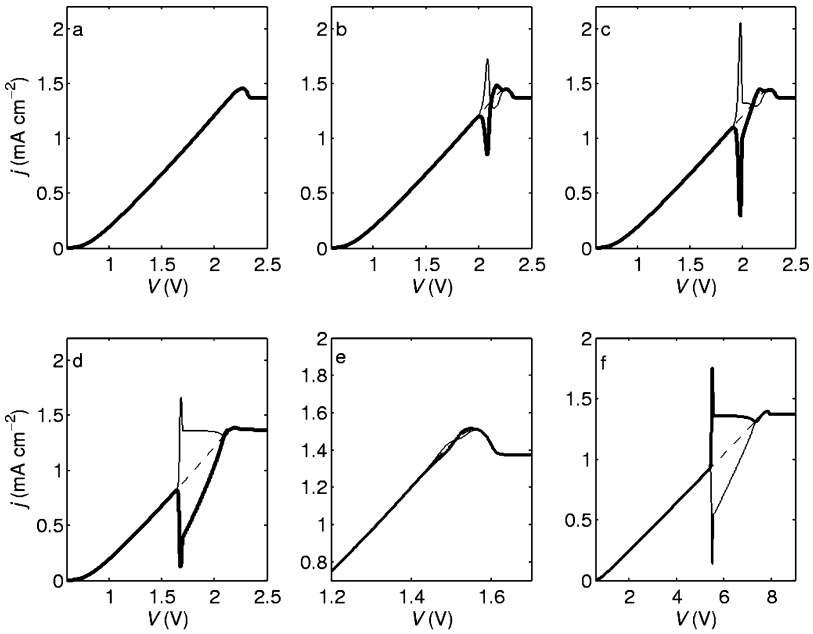

Figure 3. Numerical simulations of forward polarization scans of two (identical) electrodes with coupling. (*Top row*) Effect of coupling strength, ϵ (K). $R_{eq} = 1000\ \Omega$, scan rate = 50 mV/s. (a) $\epsilon = 0.991$ ($K = 0.11\ \Omega^{-1}\ cm^{-2}$). (b) $\epsilon = 0.995$ ($K = 0.2\ \Omega^{-1}\ cm^{-2}$). (c) $\epsilon = 0.999$ ($K = 1\ \Omega^{-1}\ cm^{-2}$). (*Bottom row*) Effect of scan rate and total resistance. (d) Scan rate = 15 mV/s, $R_{eq} = 1000\ \Omega$, $\epsilon = 0.999$ ($K = 1\ \Omega^{-1}\ cm^{-2}$). (e) $R_{eq} = 500\ \Omega$, scan rate = 50 mV/s, $\epsilon = 0.998$ ($K = 1\ \Omega^{-1}cm^{-2}$). (f) $R_{eq} = 5000\ \Omega$, scan rate = 50 mV/s, $\epsilon = 0.9998$ ($K = 1\ \Omega^{-1}cm^{-2}$). Solid thick line: electrode 1. Solid thin line: electrode 2. Dashed lines show the corresponding behavior without coupling, i.e., $\epsilon = 0$ ($K = 0\ \Omega^{-1}cm^{-2}$). Initial conditions for the scans: $\{E, \Theta_{CO}, \Theta_{OH}, c_{CO}\}$ for electrode 1: {0.55 V, 0.99, 0.02, 1.1×10^{-6} mol/L}, for electrode 2 {0.45 V, 0.98, 0.01, 1×10^{-6} mol/L }.

$= NR_{tot}$ is defined. A charge balance based on the simple equivalent circuit shown in Figure 2b for a multi-electrode setup is as follows:[20]

$$C_d \frac{dE_k}{dt} = \frac{V - E_k}{R_{eq}A} - j_{F,k} + K \sum_{k=1}^{n} (E_{avg} - E_k) \qquad (9)$$

where $k = 1...N$, E_{avg} is the mean double layer potential drop, and K is the effective positive coupling:

$$K = \frac{1}{R_{eq}A} \frac{\epsilon}{1 - \epsilon} \qquad (10)$$

The equations for the other variables are simply indexed versions of eqs 1a−c. For two electrodes ($N = 2$), the current density of each electrode (j_k) is

$$j_k = \frac{P - E_k}{R_{ind}A} \qquad (11)$$

where P is the summed potential drop on the double layer and the individual resistors:

$$P = (1 - \epsilon)V + \epsilon E_{avg} \qquad (12)$$

In this paper we investigate the effect of coupling strength ϵ on the dynamics of the coupled system with two electrodes at sufficiently large resistances such that only a monostable state exists on a single electrode or on sets of electrodes without coupling.

Computational Methods. The software XPP was used in integrating the ordinary differential equations of the model with a Gear-based adaptive stiff method. This method provided consistent convergence in the solutions to the ODEs with a step size of 0.01 s and an error tolerance of 10^{-3}. Bifurcation diagrams were obtained with the built-in AUTO 97 interface of XPP.

Simulation Results. The polarization scan of two electrodes without coupling ($\epsilon = 0$) at $R_{eq} = 1000\ \Omega$ is identical to that shown Figure 1d for a single electrode. The effect of coupling on the polarization scan is demonstrated in three scans in the top row of Figure 3; the scan rate (50 mV/s) is a value that can be conveniently used in experiments. Up to $\epsilon = 0.991$ (Figure 3a), the effect of coupling is negligible. At about $\epsilon = 0.995$ (Figure 3b), the polarization scan shows that before reaching the mass-transfer limited region the current of one electrode suddenly increases while the current of the other electrode decreases. At even stronger coupling ($\epsilon = 0.999$, Figure 3c), this splitting effect is stronger: it covers a larger potential range and the differences between the currents are larger. The overshoots seen in Figures 3b and 3c are due to transient effects. In the overshoots (at about $V = 2.15$ V in Figure 3c) the high and low current states transiently switch positions. These overshoots will also be seen in the experiments as will be seen below. At a lower scan speed (15mV/s, Figure 3d) transient effects are minimized, there are no overshoots just below the mass transfer limited region, and the splitting window is larger. (Decreasing the scan speed to even lower values does not have a significant effect). The equivalent resistance also affects the intensity of the splitting behavior. At lower (Figure 3e) and larger (Figure 3f) resistances (with constant effective coupling, K) the splitting intensity is weaker and stronger, respectively.

The characteristics of the splitting behavior at strong coupling ($\epsilon = 0.999$) can be seen in the bifurcation diagrams (Figure 4) that show both stable and unstable steady states of the system as a function of fixed circuit potential V. Without interaction, the behavior is the same as that for a single electrode (Figure 1c); the current density increases almost linearly until the mass-transfer limited plateau is reached at large resistance. With

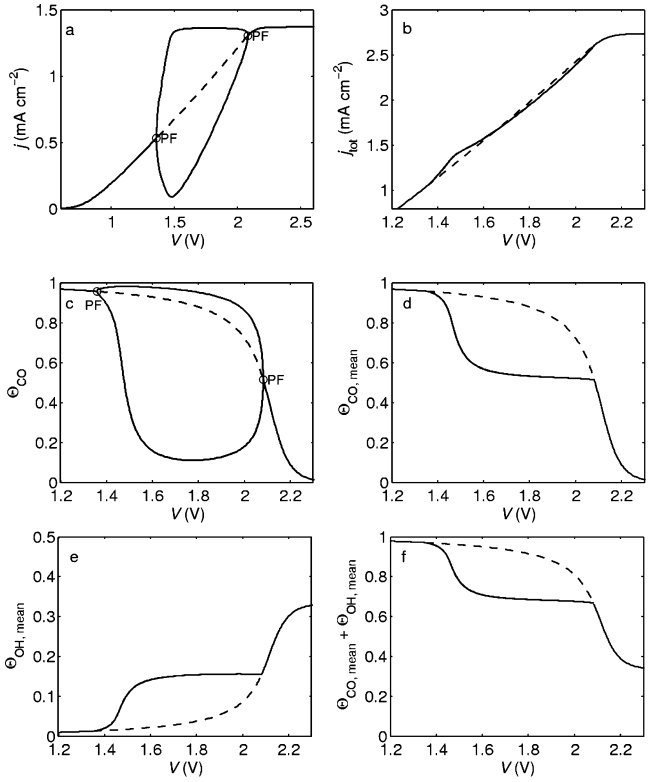

Figure 4. Numerical simulations: Bifurcation diagrams of two (identical) electrodes with coupling. $R_{eq} = 1000\ \Omega$, $\epsilon = 0.999$ ($K = 1\ \Omega^{-1}\ cm^{-2}$). (a) Bifurcation diagram showing current density of electrode 1 vs potential. (b) Total current density vs potential. (c) Bifurcation diagram showing CO coverage of electrode 1 vs potential. (d) Mean CO coverage of the two electrodes vs potential. (e) Mean OH coverage vs potential. (f) Average of the sum of CO and OH coverages vs potential. Solid line: stable steady state. Dashed line: unstable steady state. PF: pitchfork bifurcation.

coupling (Figure 4a) the same current dependence occurs although the uniform state is unstable over a range of applied circuit potential 1.36 V < V < 2.08 V; the stability is lost through two supercritical pitchfork bifurcations. At the lower pitchfork bifurcation the single stable steady state loses stability above the bifurcation point and two new stable states (one with lower, the other with larger, current density) emerge. The diagram shown is for one of the electrodes. The diagram for the other is identical except that the states are reversed; when one electrode has a high current density in the bistable region, the other has a low current. The splitting behavior seen in the scans of Figure 3 is a consequence of the stability loss of the uniform solution due to the coupling. At these parameters the splitting has only a small effect on the total current (Figure 4b); the total current is slightly increased at low potentials in the bistable region and slightly decreased at larger potentials.

Figures 4c−e show the dependence of two important chemical quantities, Θ_{CO} and Θ_{OH}, on applied circuit potential. The CO coverage without coupling is given by the monotonically decreasing solid and dotted curve in Figure 4c; the coverage of CO decreases with increasing potential due to the removal of CO of the surface at larger potentials. With coupling, due to the pitchfork bifurcation and the resulting unstable region, one electrode is highly covered with CO (producing low CO oxidation rates) while the other electrode is almost free of CO (because CO is efficiently oxidized, producing a high oxidation rate). The mean CO coverage on the two electrodes is significantly lower than the uncoupled case in a large potential region where the splitting occurs (see Figure 4d). Thus coupling

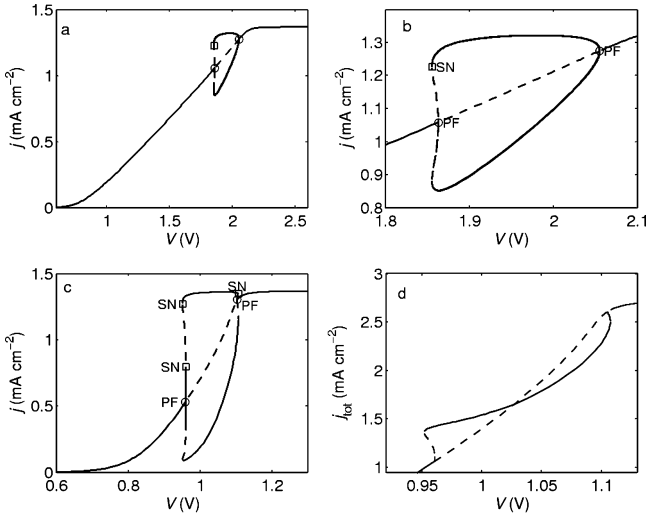

Figure 5. Numerical simulations: Bifurcation diagrams of two (identical) electrodes with coupling: the effect of coupling strength and total resistance. (a, b) Bifurcation diagram with $R_{eq} = 1000\ \Omega$, $\epsilon = 0.9091$ ($K = 0.01\ \Omega^{-1}\ cm^{-2}$). Panel b is a zoom on the bifurcation region of panel a. (c, d) Bifurcation diagram with $R_{eq} = 250\ \Omega$, $\epsilon = 0.996$ ($K = 1\ \Omega^{-1}\ cm^{-2}$). Current of electrode one and total current are shown as a function of circuit potential, V, in panels c and d, respectively. Solid line: stable steady state. Dashed line: unstable steady state. PF: Pitchfork bifurcation. SN: saddle-node bifurcation.

reduces the mean CO coverage. Similar effects are seen in OH coverage; one electrode in the bistable region has a higher OH coverage than in the uncoupled case, the other has a lower coverage; the mean OH coverage is increased due to coupling as seen in Figure 4e. The aggregate coverage of CO and OH is shown in Figure 4f; the coupling decreases the total coverage of $\Theta_{CO} + \Theta_{OH}$ in the splitting window and therefore increases the number of free active sites. The bifurcation diagrams in the variables E_1 and E_2 are similar to those shown in Figure 4 except that the differences between the high and low current states are very small.

The bifurcation diagrams shown in Figure 4 were obtained at strong coupling ($\epsilon = 0.999$). For comparison a bifurcation diagram at an intermediate coupling strength is shown in Figures 5a,b. The region of instability of the uniform state covers a smaller potential range (1.86 V < V < 2.06 V) than at stronger coupling and the current differences are smaller. In addition, the lower pitchfork bifurcation is now subcritical; the stable high and low current states are created with an additional saddle-node bifurcation.

Circuit resistance also has a significant effect on the behavior. Currents of the individual electrodes and the total current are shown in Figures 5c and 5d, respectively, at lower resistance ($R_{eq} = 250\ \Omega$). The bifurcation structure is somewhat more complicated than that obtained at $R_{eq} = 1000\ \Omega$. The first bifurcation point (at smaller V) is supercritical, but there are two additional saddle-node bifurcations at which the stable high and low current states are created; the bifurcation at large V is subcritical (similar to that shown in Figure 5b). The behavior seen here with smaller resistance differs in one significant aspect from that obtained above with large resistance: under these conditions the coupling produces large changes in the total current. The total current with pattern formation (strong coupling) differs from that of the uncoupled, uniform state. In the lower potential region of the splitting window the total current is increased, in the larger potential region it is decreased (see Figure 5d).

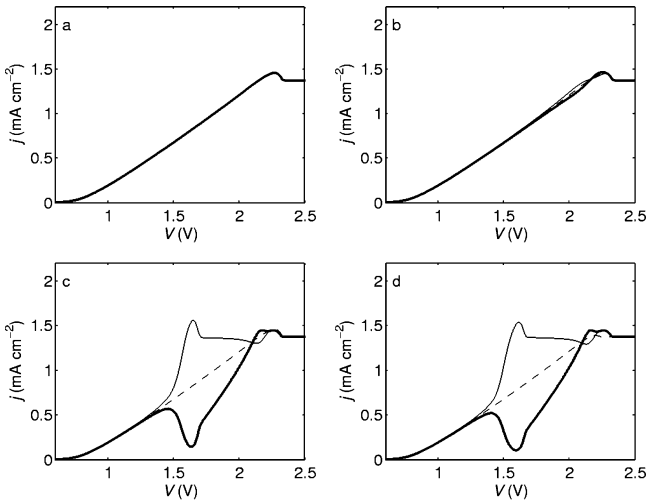

Figure 6. Numerical simulations of forward polarization scans of two nonidentical electrodes ($\sigma = 0.01$): the effect of coupling strength, ϵ (or K). $R_{eq} = 1000\ \Omega\ cm^{-2}$, scan rate = 50 mV/s. (a) $\epsilon = 0$ ($K = 0\ \Omega^{-1}\ cm^{-2}$). (b) $\epsilon = 0.9091$ ($K = 0.01\ \Omega^{-1}\ cm^{-2}$). (c) $\epsilon = 0.991$ ($K = 0.11\ \Omega^{-1}\ cm^{-2}$). (d) $\epsilon = 0.999$ ($K = 1\ \Omega^{-1}\ cm^{-2}$). Dashed lines in panels b−d represent the behavior of electrode 1 in the uncoupled case [$\epsilon = 0$ ($K = 0\ \Omega^{-1}\ cm^{-2}$)]. Solid thick line: electrode 1. Solid thin line: electrode 2.

At large resistance ($R_{eq} = 5\ k\Omega$) the bifurcation diagram is similar to that shown with $R_{eq} = 1\ k\Omega$ (Figure 4a) but the region of instability of the uniform state extends over a larger circuit potential due to the increased potential drop on the external resistors. The effect of the coupling on total current is, however, almost negligible.

Effect of Heterogeneities. In laboratory experiments there are always some heterogeneities on surfaces; in the present case this arises as unavoidable differences between the electrodes. Even small heterogeneities can affect the dynamical behavior of the system. Heterogeneities are simulated in our model by using slightly different CO adsorption rates of the two electrodes: $k_{CO,ads}(1,2) = k_{CO,\ ads}\ (1 \pm \sigma)$, where σ is a heterogeneity parameter. Changes in CO adsorption rates can, for example, model different compositions of the polycrystalline surface of the two electrodes. Here we consider $\sigma = 0.01$, i.e., the CO adsorption rate for electrode one is 1% larger, for electrode 2 is 1% smaller than the nominal value.

In Figure 6 the effect of changes in the coupling parameter ϵ is investigated at a fixed value of the heterogeneity parameter σ. The degree of heterogeneity is small such that without any coupling, the small heterogeneity has a negligible effect on the polarization scan with large resistance (see Figure 6a); electrode one (with larger k_{CO}) has about 0.1% smaller current throughout the scan. As the coupling strength is increased, the effect of the heterogeneity becomes more pronounced. At $\epsilon = 0.9091$ (Figure 6b), a small split is seen and at somewhat larger coupling strengths ($\epsilon = 0.991$, Figure 6c; and $\epsilon = 0.999$, Figure 6d) a split with full intensity occurs. The heterogeneities play a major role; under similar conditions (but without heterogeneities) splits are either not observed (Figure 3a) or can only be obtained with smaller scan speed (Figure 3d). There is also a difference in the start of the split on the polarization scan: without heterogeneity the split is abrupt, with heterogeneity it is smoother.

Additional effects of heterogeneities can be seen in Figures 7a−c (scans) and Figures 7d,e (fixed values of V). The heterogeneities cause the electrodes to split toward the high or low current state consistently, independently of the initial conditions. Without heterogeneities (because of the symmetry

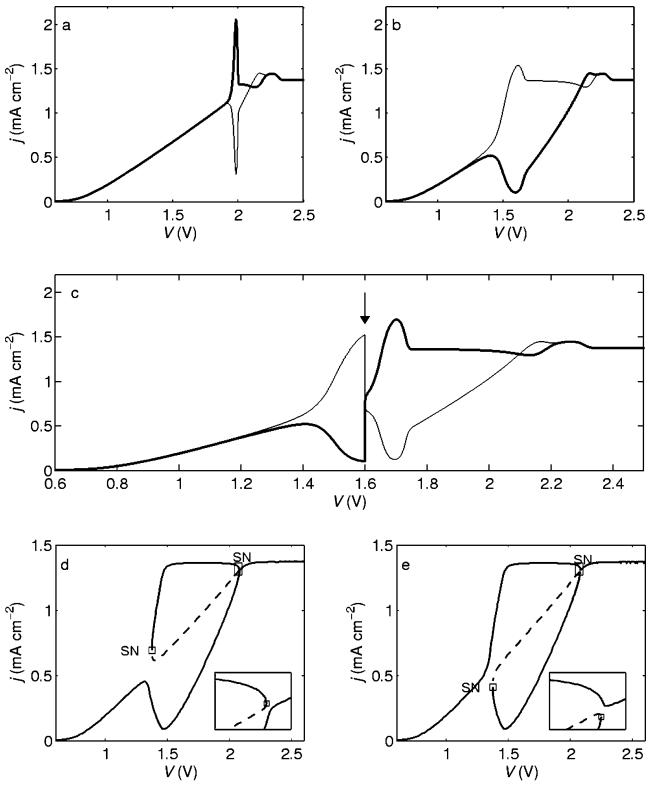

Figure 7. Numerical simulations: Polarization scans and bifurcation diagrams of two coupled electrodes: the effect of heterogeneities. (a) Forward polarization scan of two identical electrodes ($\sigma = 0$) with the same conditions as in Figure 3c but with switched initial conditions for the two electrodes. Solid thick line: electrode 1. Solid thin line: electrode 2. (b) Forward polarization scan of two nonidentical electrodes ($\sigma = 0.01$) with the same conditions as in Figure 6d but with switched initial conditions for the two electrodes. Solid thick line: electrode 1. Solid thin line: electrode 2. (c) The same scan as in panel b, but at $V = 1.6$ V (shown by the arrow) the variables for electrode 2 were changed to conditions [$\{E, \Theta_{CO}, \Theta_{OH}, c_{CO}\} = \{0.45$ V, 0.98, 0.01, 1×10^{-6} mol/L$\}$] simulating a change to open circuit, i.e., close to those obtained at $V = 0.6$. (d) Bifurcation diagram of two nonidentical ($\sigma = 0.01$) electrodes showing the current of electrode 1 as a function of circuit potential, V. $R_{eq} = 1000\ \Omega\ cm^{-2}$, (a) $\epsilon = 0.999$ ($K = 1\ \Omega^{-1}\ cm^{-2}$). Solid line: stable steady state. Dashed line: unstable steady state. SN: saddle-node bifurcation. Inset: a zoom on the SN bifurcation at larger V. The size of the rectangle in the main panel corresponds to the scaling of the inset. (e) Same as in panel d but for electrode 2.

of the ODEs) if initial conditions for electrode 1 and 2 are switched, the electrodes following the high and the low current path will be switched as well (compare Figures 3c and 7a). However, with heterogeneities, such a switch does not affect the current path of the electrodes (compare Figures 6d and 7b). The electrode with larger value of $k_{CO,ads}$ has a tendency to follow the low current path in the scan. However, with a well-timed perturbation a switch between the low and large current state can be initiated. In Figure 7c, at $V = 1.6$ V the state of electrode 2 (thin line) was set to its initial conditions; such a change can simulate in the experiments a break of the current circuit. As a result the large current of electrode 2 dropped and after a short transient electrode one followed the low current path in the scan.

These observations can be explained by analyzing the bifurcation diagram of electrode 1 and 2, shown in Figures 7d and e, respectively. Because of the loss of the symmetry in the system, the pitchfork bifurcations seen in the nonheterogeneous case disappear and an isola is formed. With increases in the circuit potential, electrode one follows a low current branch

without any bifurcations. The large-current branch is an isola that is formed by two saddle-node bifurcations. For electrode 2 (Figure 7e), the isola is a low current branch. Therefore, during a scan electrodes 1 and 2 follow low and high current paths, respectively; however, in the isola region the two states can be switched by a proper perturbation.

3. Experiments

Procedures. The experiments were carried out in a three-electrode electrochemical cell schematically shown in Figure 2a. Solutions of 0.05 mol/L H_2SO_4, 0.05 mol/L H_2SO_4 + sat. Na_2SO_4, or 0.10 mol/L $HClO_4$ were used as cell electrolytes. A gas sparger was used to introduce CO (Messer, 99.99%) or 2% CO/H_2 (Messer, Scientific Grade) gases to the cell; the sparger was positioned near the wall to minimize turbulence. The counter electrode was a platinum-clad niobium expanded-mesh. The reference electrode was a Hg/Hg_2SO_4/sat. K_2SO_4 electrode; all potentials reported here are with respect to a standard hydrogen electrode. Two polycrystalline platinum disks (ESPI Inc, 99.99%) of 4.7625 mm diameter in 14.3 mm distance were used as a working electrode; the electrodes were embedded in epoxy and reaction takes place only at the ends. The potential of the working electrode was controlled by a potentiostat (Pine Model AFCBP1). The current was measured with zero-resistance ammeters. The measured currents and the potential were digitized at a rate of 100 Hz with a DAS-1802HC digital analogue converter.

Before each set of experiments, the surfaces of the electrodes were polished with 1 and 0.05 μm Buehler Micropolish alumina. The electrodes were then sonicated for 15 min in distilled water to remove any residual polishing material. The electrodes were electrochemically cleaned for 20 min by 350 mV/s continuous potential sweeps between −0.15 and 1.75 V in 0.05 mol/L H_2SO_4. The cell electrolyte was purged with N_2 gas for at least 20 min to remove dissolved oxygen. The solution was then saturated with CO (or CO/H_2) gas until open cell equilibrium potentials reached a steady value, approximately 0.25 and 0.05 V, respectively. After the current level decreased below 0.1 μA at these potentials (indicating that the surface was covered with CO), the gas flow rate was minimized to reduce turbulence in the system from bubbling and potential scans were carried out at a scan speed of 50 mV/s.

Behavior of a Single Electrode. Cyclic polarization scans of CO oxidation on a single polycrystalline Pt electrode in three different electrolytes, 0.05 mol/L H_2SO_4 + sat. Na_2SO_4, 0.05 mol/L H_2SO_4, and 0.10 mol/L $HClO_4$ solutions are shown in Figures 8 a−c, respectively. In sulfuric acid and perchloric acid electrolytes, bistability has been seen during CO oxidation on Pt single crystals due to the S-shaped polarization curve.[5,6] On the polycrystalline electrodes used in this investigation, bistability is most clearly seen in the 0.05 mol/L H_2SO_4 + sat. Na_2SO_4 solution (Figure 8a). The forward and backward scans are very similar to those of the numerical simulations (Figure 1b); they exhibit an oxidation peak at about 0.86−0.87 V and bistability between about 0.78 and 0.86 V. The model does not account for two details of the experiments. First, in the experiments the current decreases above the oxidation peak rather than leveling out on a mass-transfer limited current plateau. The decrease of current is due to the combined effect of oxide formation[7,21] and sulfate adsorption.[6] (Because of the formation of this oxide a reduction peak appears in the backward scan at about 0.5−0.6 V. This peak is typically small at a reasonably high scan rate of 50 mV/s as in Figure 8.) Second, a prewave occurs (very small in Figure 8) at about 0.65 V; this

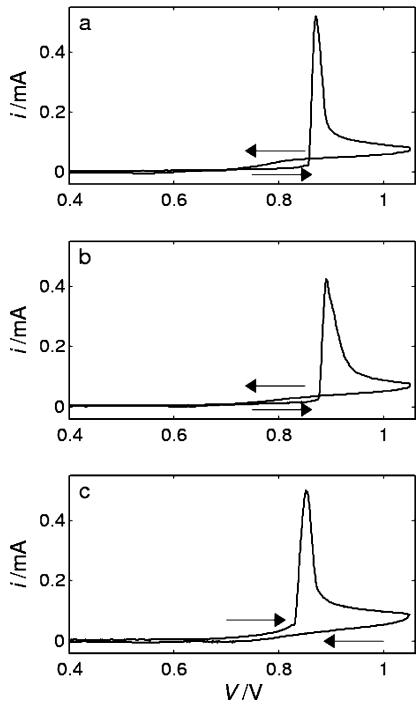

Figure 8. Experiments on CO oxidation: CV scans of a single electrode in different electrolytes. (a) 0.05 mol/L H_2SO_4 + sat. Na_2SO_4. (b) 0.05 mol/L H_2SO_4. (c) 0.1 mol/L $HClO_4$. Scan rate: 50 mV/s, $R_{eq} = 0\ \Omega$.

prewave is due to CO oxidation through an alternative pathway in which there is no self-inhibition of CO and in which the reaction order in CO is positive.[5] (We do not investigate the effect of coupling in the prewave region and it is not included in the model.) In sulfuric acid (Figure 8b), the bistability region is smaller; in perchloric acid (Figure 8c) clear bistability was not found. Thus in the three solutions with different sulfate concentrations the extent of bistability is different. Sulfate and bisulfate ions are known to interact strongly with a platinum surface; they have the strongest interaction with Pt(111).[1] The anions change the resistivity of the electrolyte and also can affect the kinetic parameters such as by changing the crystal configuration [1].

Experimental Results on Coupled Electrodes. We now explore the effect of coupling in the two-electrode system with the three electrolytes. Results are first given for the 0.05 mol/L H_2SO_4 + sat. Na_2SO_4 solution in which the bistability without added resistance is the strongest.

Polarization (forward) scans of two electrodes as a function of coupling strength are shown in Figures 9a−e; the circuit resistance is large ($R_{eq} = 4\ k\Omega$, $\epsilon = 0$). Figure 9a was obtained without coupling in which case the two electrodes behave similarly; there are small differences at low (below 0.9 V) and large potentials (above 1.2 V). Differences between the two curves are largely due to heterogeneities or differences between the surfaces of the two electrodes. (The scans of the single electrodes are practically identical to those shown in Figure 9a.) The current remains low until about 0.9 V, above which it almost linearly increases (ohmic region). There is no sudden change of current indicating an absence of bistability; the forward polarization scan is similar to those obtained in the simulations except for the current decrease due to oxide formation at larger potentials. A reduction peak (reduction of the oxides) occurs in the reverse scan (not shown) at about 0.5 V.

Figures 9b through 9e show the effect of coupling, ϵ. Up to $\epsilon = 0.5$ only small differences in the currents can be observed

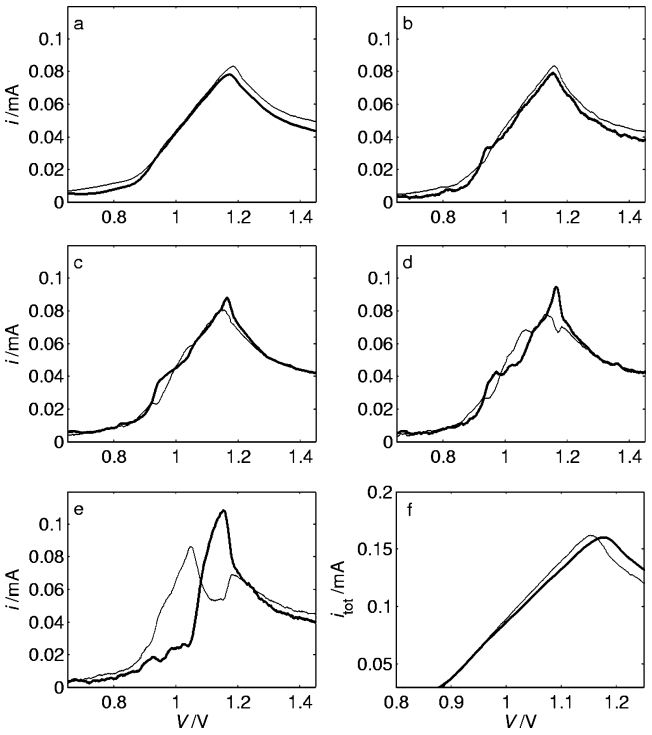

Figure 9. Experiments on CO oxidation: effect of coupling strength on forward CV scans of two electrodes in 0.05 mol/L H_2SO_4−sat. Na_2SO_4 electrolyte. $R_{eq} = 4$ kΩ. (a) Without added coupling, $\epsilon = 0$. Thick line: electrode 1. Thin line: electrode 2. (b) $\epsilon = 0.5$. (c) $\epsilon = 0.75$. (d) $\epsilon = 0.95$. (e) Maximum added coupling, $\epsilon = 1$. (f) Total current during the forward scan. Thick line: $\epsilon = 1$. Thin line: $\epsilon = 0$.

(Figure 9b). For somewhat larger values, $\epsilon = 0.75$ and 0.95, there are two changes; the currents of the two electrodes become closer at large and small potentials but in an intermediate region ($0.9\ V < V < 1.2\ V$) small differences begin to arise. With maximum added coupling ($\epsilon = 1$, Figure 9e) there is a dramatic change in the polarization scans. In the ohmic region, where without interactions the currents of the electrodes are identical, a splitting is observed in which electrode one (thick line) follows initially a large current path while electrode two follows a low one. Above $V = 1.1$ V, the positions are switched. These experimental results show the same splitting behavior as in the numerical simulations with small heterogeneities (see Figure 6d). In the experiments, the second, "overshoot splitting", is larger than in the simulations indicating stronger transient effects. It seems that well-developed splitting can be experimentally observed only for coupling strength $\epsilon > 0.95$. These results are consistent with the simulation findings that showed (Figure 6) that the splitting behavior develops at large coupling strengths.

(The backward scans (not shown for clarity) do not exhibit any splitting at these conditions but the split in the backward scan does occasionally appear, particularly with the other electrolytes. The simulations do show splits in both scan directions. The chemistry is apparently very different in the backward scan, perhaps due to the oxides.)

A comparison of the total currents at $\epsilon = 0$ and $\epsilon = 1.0$ is shown in Figure 9f; only the potential window in which splitting occurs is presented. At $\epsilon = 1.0$, the total current is slightly smaller than that without coupling above approximately $V = 1.0$ V; this is consistent with the numerical findings that the effect of coupling on total current is small when the circuit resistance is large (see, e.g., Figure 4b).

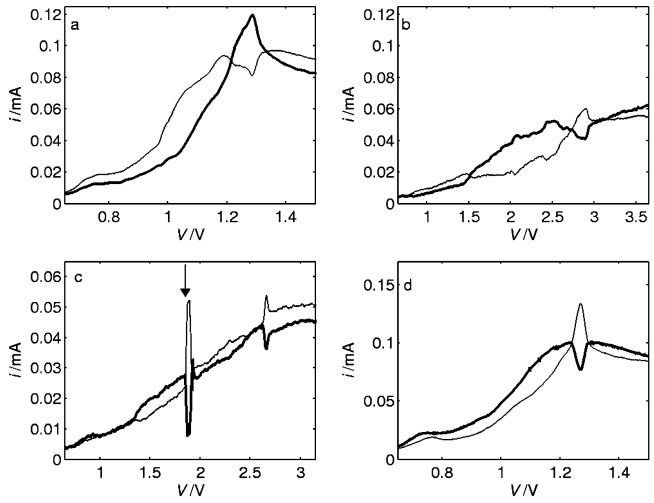

Figure 10. Experiments on CO oxidation in different electrolytes. Forward CV scans of the two-electrode setup with maximum added coupling, $\epsilon = 1$. (a−c) 0.05 mol/L H_2SO_4, (a) $R_{eq} = 4$ kΩ. (b) $R_{eq} = 40$ kΩ. (c) $R_{eq} = 40$ kΩ with perturbation. Electrode 1 (thick line) was briefly disconnected during the scan (at about $V = 1.25$ V denoted by the arrow) while electrode 2 (thin line) remained connected. (d) 0.1 mol/L $HClO_4$. $R_{eq} = 4$ kΩ. Scan speed: 50 mV/s.

The reproducibility of the splitting is very good. In repeating scans at a fixed coupling strength without repolishing the surface or increasing the electrode potential to very large values into the oxide formation region, the same electrodes always follow the high and low current path and the shapes of the splitting currents are similar. If these conditions are not satisfied (for example, if the electrode is re-polished), however, the splitting still occurs but the splitting intensity and waveform can be different. Experiments at smaller equivalent resistance (results not presented) show that in accordance with the numerical simulations, the splitting intensity at the same coupling strength and scan speed is smaller with smaller R_{eq}.

Representative experiments in 0.05 mol/L H_2SO_4 are shown in Figure 10a−d. At $R_{eq} = 4$ kΩ, the scans without coupling ($\epsilon = 0$) are similar to those in 0.05 mol/L H_2SO_4 + sat. Na_2SO_4. With maximum added coupling ($\epsilon = 1$, Figure 10a) splitting can be observed; however, its intensity is smaller than those in electrolytes with large sulfate content seen in Figure 9e. With a very large resistance ($R_{eq} = 40$ kΩ, Figure 10b) the splitting can be clearly seen; this indicates that the splitting will also likely occur in galvanostatic operation since the galvanostatic mode of operation is similar to running the cell at large R_{eq} and ϵ.

A perturbation experiment similar to that done in the numerical simulations (Figure 7c) is shown in Figure 10c to explore the capability of the system to switch between the high and low current paths at strong coupling. Without perturbation (Figure 10b) electrode 1 (thick line) initially follows the high current path. A perturbation was introduced by breaking the circuit path for electrode 2 in the splitting region. When the perturbation is applied at the appropriate potential for long enough time (Figure 10c), the states could be switched and the currents of the electrodes followed the alternate current path. (In Figure 10c the differences between the two electrodes caused by coupling is smaller than in 10b, likely due to changes in surface properties; nevertheless, the qualitative feature of switching is the same as that seen in the simulations, Figure 7c.)

Experiments with 0.01 mol/L $HClO_4$ are shown in Figure 10d with maximum added ($\epsilon = 1$) coupling. Without coupling,

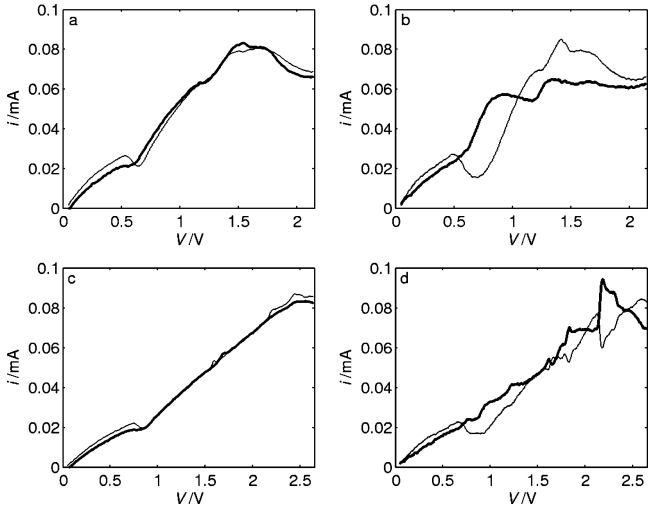

Figure 11. Experiments on CO/H_2 oxidation: Forward CV scans of 2% CO−98% H_2 mixtures in a two-electrode setup with and without coupling in 0.05 mol/L H_2SO_4. (a) Without added coupling, $\epsilon = 0$, $R_{eq} = 10$ kΩ. (b) Maximum added coupling, $\epsilon = 1$, $R_{eq} = 10$ kΩ. (a) Without added coupling, $\epsilon = 0$, $R_{eq} = 20$ kΩ. (b) Maximum added coupling, $\epsilon = 1$, $R_{eq} = 20$ kΩ. Thick line: electrode 1. Thin line: electrode 2. Scan speed: 50 mV/s.

the scans are similar to those in the sulfuric acid experiments but there is a larger prewave at about $V = 0.75$ V. With coupling, the intensity of splitting is weaker than that with sulfate electrolytes. The current difference between the two electrodes is smaller but a well-developed secondary overshoot peak can be observed. These two features are characteristics of the scans in perchloric acid in a wide range of the studied equivalent resistance 1 kΩ $< R_{eq} <$ 20 kΩ. Thus, even though clear bistable behavior is not found on a single electrode, the splitting is seen with two electrodes.

The splitting behavior can also be observed during the simultaneous oxidation of CO and H_2. H_2 is oxidized very fast on the surface sites not covered by CO or OH.[1] Thus, when patterns form on the electrode array due to CO oxidation, the differences in currents can be intensified by large H_2 oxidation currents. The idea was tested on 2% CO/H_2 gas in which (on single crystals) an S-shaped polarization curve without added resistance has been previously observed.[2] In the two-electrode configuration studied here, a larger equivalent resistance ($R_{eq} > 4$ kΩ) was required compared to the pure CO case to obtain an almost linear ohmic region on the scans without added coupling ($\epsilon = 0$, see Figures 11ac). With maximum added coupling ($\epsilon = 1$), splitting behavior does appear with both the smaller ($R_{eq} = 10$ kΩ, Figure 11b) and larger ($R_{eq} = 20$ kΩ, Figure 11d) equivalent resistances.

4. Discussion

It is seen through both experiments and simulations that large differences in the currents on Pt electrodes occur during CO electro-oxidation as the coupling strength between two electrodes is increased. Furthermore, simulations show that such differences can arise even on identical surfaces since variations are produced by the symmetry breaking.

Inherent nonuniformity or heterogeneity, due to differences of kinetic parameters, can also occur in surface reactions due to variations in local surface properties. These may develop in the course of an experiment by some pretreatment, or may be due to a variation of the local density of the catalyst, porosity, catalyst thickness, nonuniformities of the temperature distribution in the reactor, or imperfect mixing in the fluid phase (see ref 22 and references therein). The presence of positive coupling among the reaction sites (typically through the temperature, pressure, or potential field) usually effectively reduces these heterogeneities; the addition of positive coupling then results in a more uniform spatial activity. For example, it has been shown that coupling can synchronize the oscillation frequencies of a heterogeneous population of electrodes.[18] In this present paper, the activity of two Pt electrodes during electrocatalytic CO oxidation was investigated in laboratory experiments and numerical simulations with tuned positive interactions. In the presence of strong coupling, the interactions can initiate nonuniform activities in which one electrode exhibits a high reaction rate while the other is practically inactive. The different activities of the two electrodes are remarkable since catalytic activities are mostly influenced by surface structure, catalyst material, temperature, applied driving force of the reaction, etc., each of which is similar in our case for the two electrodes as confirmed by measurements without interactions. Although patterns can develop on identical electrodes with interactions, it is seen that small inherent heterogeneity has a major effect on the resulting state; the nonuniform reaction rates due to heterogeneities are greatly amplified by coupling.

The experiments were carried out with carefully tuned coupling strengths. The mechanism of the observed symmetry breaking due to coupling is very similar to that in the formation of Turing patterns in distributed systems. On the basis of our results, we expect similar symmetry breaking transitions to be seen in larger sets of reaction sites and also on distributed systems. Experiments with eight globally coupled electrodes show results similar to those obtained in this paper;[23] although the transitions are more complicated, symmetry breaking does occur in a region of circuit potential in which sets of electrodes exhibit large activities while others are practically inactive. Turing structures have also previously been seen in a continuous electrochemical system.[7] A nonuniform potential distribution was observed on a rotating polycrystalline Pt ring during CO electro-oxidation in a dilute (2×10^{-3} mol/L) perchloric acid solution. A dilute solution with low conductivity was used to produce a large ohmic drop in the electrolyte so that an external resistance was not required; long-range coupling is inherent in the system and is determined by the cell geometry. The potential distribution on the ring exhibited three peaks and rather small amplitudes (about 15 mV) in a circuit potential window.

Our findings in the two-electrode systems support and augment the results on Turing-type patterns on a ring. It was shown that the patterns develop from the nearly uniform current distribution with increased coupling. Our setup also enables us to measure the currents directly on the electrodes; it was found that although the amplitudes of the potential patterns are small, variations in other observable variables including current and concentrations (or coverages) of chemical species can be quite large because of the coupling.

In general, the stronger the coupling, the larger the extent of the pattern formation observed. Thus, in CO oxidation the extent of stationary patterning can be tuned between the uniform and large amplitude asymmetric case; the experimental setup enables the creation of a structured active area with varying uniformity. Patterns were also observed at very large resistances; since running an electrochemical cell at large (series) resistance simulates a galvanostatic mode of operation, the patterns are also expected to form under galvanostatic control.

Simulations show that the symmetry breaking produces patterned states in which the total coverage of CO and OH is always lower and thus the number of total free active sites is

higher than in the corresponding uniform state. Moreover, at low total resistance and quasi-stationary circuit potential (low scan rates), changes up to 20% in total current can occur. This opens up a possibility of increased reactivity not only in the CO oxidation system but also in systems in which CO electro-oxidation occurs in parallel with other chemical and electrochemical reaction steps on the free sites. In these cases, running the experiments under conditions favorable for pattern formation could have a beneficial effect on the total reaction rate.

The experiments were carried out in three different electrolytes exhibiting different extent of S-shaped polarization curves; all three electrolytes exhibited pattern formation with strong coupling. The sulfate-saturated sulfate electrolyte exhibited both the strongest bistability and the most pronounced pattern formation; parallel tendencies in exhibited bistability and pattern formation characteristics were seen in the three electrolytes, sulfate-saturated sulfuric acid > sulfuric acid > perchloric acid. (The sulfate ions affect the cell dynamics in several ways: they induce surface changes and kinetic features responsible for bistability as well as changes in electrolyte resistivity.) Since stationary pattern formation requires bistability (S-shaped polarization curve) at small ohmic drops, it is reasonable that systems with stronger bistability would also show stronger pattern formation.

A numerical bifurcation analysis of coupled ODE models of CO electro-oxidation revealed that when the two electrodes are identical the high and low activity states are created through pitchfork bifurcations. The bifurcation can be sub- or supercritical depending on the coupling strength and total resistance. Whether the specific electrode follows the high or the low activity region is determined by the initial conditions. With a small amount of heterogeneities there is a change in the bifurcation diagram. In simple scans of the circuit potential the electrode with higher affinity for CO follows low, with lower affinity, the high current path without any bifurcations. The alternate pathway is located on an isola, therefore it cannot be reached through scans; however, transitions between the low and high current states can be initiated with appropriate perturbations. The experiments confirmed the existence of isolas; transitions to states not attainable in the scans could be attained via perturbations.

CO oxidation is also a sub-process in the oxidation of small organic substances such as in formic acid oxidation;[24] it is also a side reaction in H_2 oxidation in the presence of CO that can result in voltage losses on fuel cell anodes.[25] It is possible that the pattern-forming affinity of CO oxidation reaction affects these other reaction systems. In the experiments we demonstrated that patterns similar to those in CO oxidation can form in 2% CO/H_2 mixtures. Although the current is mainly due to H_2 oxidation on the free sites, the presence of CO still produces nonuniformities and large difference in activities of the two electrodes.

We showed that electrical interactions (for example, due to a load resistance) cause large differences in activities of Pt disks, that otherwise have the same inherent catalytic activities, during the electro-oxidation of CO and CO/H_2 mixtures. The large impact of coupling on local activities implies that care must be taken in interpreting experiments in, for example, automated catalyst design with arrays when coupling and positive feedback kinetic mechanisms exist.

Acknowledgment. This work was supported in part by the National Science Foundation (CTS-0317762). We thank Gerhard Ertl for his many years of inspiration, support, and gracious hospitality.

References and Notes

(1) Markovic, N. M.; Ross, P. N., Jr. *Surf. Sci. Rep.* **2002**, *45*, 117.
(2) Markovic, N. M.; Grgur, B. N.; Lucas, C. A.; Ross, P. N. *J. Phys. Chem. B* **1999**, *103*, 487.
(3) Gasteiger, H. A.; Markovic, N. M.; Ross, P. N. *J. Phys. Chem.* **1995**, *99*, 8290.
(4) Gasteiger, H. A.; Markovic, N. M.; Ross, P. N. *J. Phys. Chem.* **1995**, *99*, 16757.
(5) Markovic, N. M.; Lucas, C. A.; Grgur, B. N.; Ross, P. N. *J. Phys. Chem. B* **1999**, *103*, 9616.
(6) Koper, M. T. M.; Schmidt, T. J.; Markovic, N. M.; Ross, P. N. *J. Phys. Chem. B* **2001**, *105*, 8381.
(7) Bonnefont, A.; Varela, H.; Krischer, K. *ChemPhysChem* **2003**, *4*, 1260.
(8) Turing, A. M. *Philos. Trans. R. Soc. B London* **1952**, *237*, 37.
(9) Castets, V.; Dulos, E.; Boissonade, J.; DeKepper, P. *Phys. Rev. Lett.* **1990**, *64*, 2953.
(10) Lengyel, I.; Kádár, S.; Epstein, I. R. *Science* **1993**, *259*, 493.
(11) Vanag, V. K.; Epstein, I. R. *Phys. Rev. Lett.* **2001**, *87*, 228301.
(12) Krischer, K. Principles of temporal and spatial pattern formation in electrochemical systems. In *Modern Aspects of Electrochemistry*; Conway, B. E., Bockris, O. M., White, R. E., Eds.; Kluwer Academic/Plenum Press: New York, 1999; Vol. 32, p 1.
(13) Krischer, K.; Mazouz, N.; Flatgen, G. *J. Phys. Chem. B* **2000**, *104*, 7545.
(14) Mazouz, N.; Krischer, K. *J. Phys. Chem. B* **2000**, *104*, 6081.
(15) Li, Y. J.; Oslonovitch, J.; Mazouz, N.; Plenge, F.; Krischer, K.; Ertl, G. *Science* **2001**, *291*, 2395.
(16) Otterstedt, R. D.; Jaeger, N. I.; Plath, P. J.; Hudson, J. L. *Chem. Eng. Sci.* **1999**, *54*, 1221.
(17) Kiss, I. Z.; Zhai, Y.; Hudson, J. L. *Phys. Rev. Lett.* **2002**, *88*, 238301.
(18) Kiss, I. Z.; Zhai, Y. M.; Hudson, J. L. *Science* **2002**, *296*, 1676.
(19) Wang, W.; Kiss, I. Z.; Hudson, J. L. *Phys. Rev. Lett.* **2001**, *86*, 4954.
(20) Kiss, I. Z.; Wang, W.; Hudson, J. L. *J. Phys. Chem. B* **1999**, *103*, 11433.
(21) Conway, B. E.; Barnett, B.; Angersteinkozlowska, H.; Tilak, B. V. *J. Chem. Phys.* **1990**, *93*, 8361.
(22) Liauw, M. A.; Plath, P. J.; Jaeger, N. I. *J. Chem. Phys.* **1996**, *104*, 6375.
(23) Brackett, A. W. Symmetry Breaking in Electro-oxidation of CO on Platinum. Master's Thesis, University of Virginia, 2004.
(24) Strasser, P.; Eiswirth, M.; Ertl, G. *J. Chem. Phys.* **1997**, *107*, 991.
(25) Carrette, L.; Friedrich, K. A.; Stimming, U. *ChemPhysChem* **2000**, *1*, 162.